AD-A041 041 VISIDYNE INC BURLINGTON MASS F/G 18/3
WILSON CLOUD FORMATION BY LOW ALTITUDE NUCLEAR EXPLOSIONS, (U)
FEB 75 R E WALTZ F19628-C-74-0207
UNCLASSIFIED VI-292 AFGL-TR-77-0016 NL

1 OF 1
AD A041041

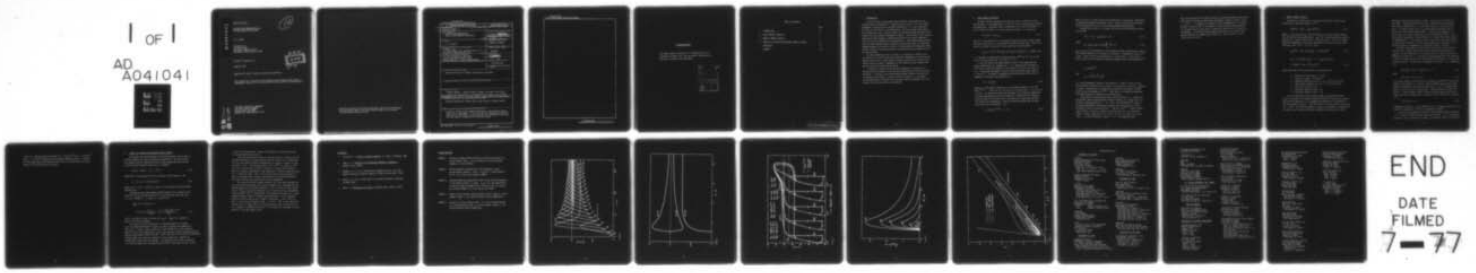

END
DATE FILMED
7-77

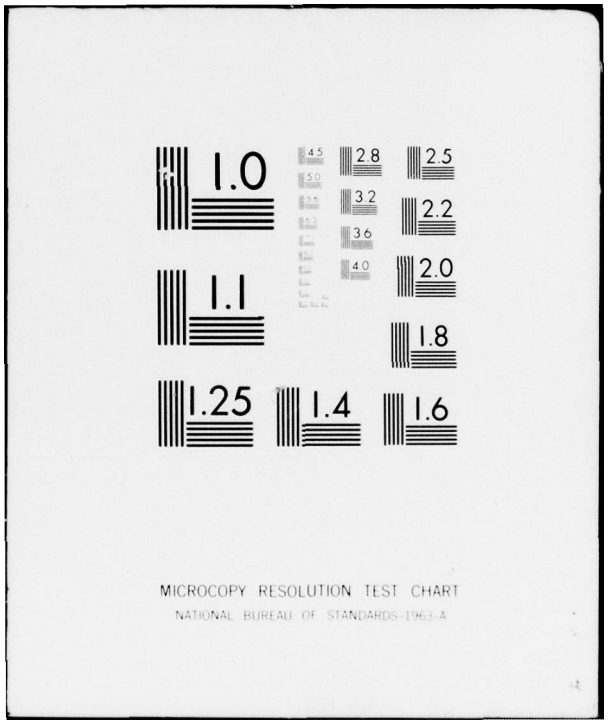
1.0
1.1
1.25
1.4
1.6
1.8
2.0
2.2
2.5
2.8
3.2
3.6
4.0
4.5
5.0
5.6
MICROCOPY RESOLUTION TEST CHART
NATIONAL BUREAU OF STANDARDS-1963-A

AFGL-TR-77-0016

WILSON CLOUD FORMATION BY LOW ALTITUDE NUCLEAR EXPLOSIONS

R. E. Waltz

Visidyne, Inc.
19 Third Avenue
Northwest Industrial Park
Burlington, Massachusetts 01803

Scientific Report No. 8

February 1975

Approved for public release; distribution unlimited.

This research was sponsored by the Defense Nuclear Agency under Subtask S99QAXHI004, Work Unit 11, entitled "OPTIR" Code and Aircraft Measurements".

AIR FORCE GEOPHYSICS LABORATORY
AIR FORCE SYSTEMS COMMAND
UNITED STATES AIR FORCE
HANSCOM AFB, MASSACHUSETTS 01731

Unclassified

SECURITY CLASSIFICATION OF THIS PAGE (When Data Entered)

REPORT DOCUMENTATION PAGE	READ INSTRUCTIONS BEFORE COMPLETING FORM
1. REPORT NUMBER: AFGL-TR-77-0016	2. GOVT ACCESSION NO.
3. RECIPIENT'S CATALOG NUMBER	
4. TITLE (and Subtitle): WILSON CLOUD FORMATION BY LOW ALTITUDE NUCLEAR EXPLOSIONS	5. TYPE OF REPORT & PERIOD COVERED: Scientific Report No. 8
6. PERFORMING ORG. REPORT NUMBER: VI-292	
7. AUTHOR(s): R. E. Waltz†	8. CONTRACT OR GRANT NUMBER(s): F19628-C-74-0207
9. PERFORMING ORGANIZATION NAME AND ADDRESS: Visidyne, Inc. 19 Third Avenue, N.W. Industrial Park Burlington, Massachusetts 01731	10. PROGRAM ELEMENT, PROJECT, TASK AREA & WORK UNIT NUMBERS: CDNA072G
11. CONTROLLING OFFICE NAME AND ADDRESS: Air Force Geophysics Laboratory Hanscom AFB, Massachusetts 01731 Contract Monitor: H.A.B. Gardiner/OPR	12. REPORT DATE: February 1975
	13. NUMBER OF PAGES: 24
14. MONITORING AGENCY NAME & ADDRESS (if different from Controlling Office)	15. SECURITY CLASS. (of this report): Unclassified
	15a. DECLASSIFICATION/DOWNGRADING SCHEDULE

16. DISTRIBUTION STATEMENT (of this Report)

Approved for public release; distribution unlimited

17. DISTRIBUTION STATEMENT (of the abstract entered in Block 20, if different from Report)

18. SUPPLEMENTARY NOTES

†Present Address: General Atomic Company, San Diego, California.

This research was sponsored by the Defense Nuclear Agency under Subtask S99QAXHI004, Work Unit 11, entitled "OPTIR" Code and Aircraft Measurements".

19. KEY WORDS (Continue on reverse side if necessary and identify by block number)

Nuclear Detonations, Wilson Cloud, Shock Physics, Aerosol Growth.

20. ABSTRACT (Continue on reverse side if necessary and identify by block number)

A model of Wilson Cloud formation following a low-altitude nuclear detonation is developed. It is shown that for detonation yields between 10^{-3} kt and 100 kt, simple scaling laws characterize the evolution and physical properties of the Wilson Cloud.

0.001

DD FORM 1 JAN 73 1473 EDITION OF 1 NOV 65 IS OBSOLETE

Unclassified

SECURITY CLASSIFICATION OF THIS PAGE (When Data Entered)

390 862

ACKNOWLEDGEMENTS

The author wishes to thank Dr. O.P. Manley and Dr. R.C. Englade of Visidyne, Inc. for many useful discussions on the topic of Wilson Cloud formation.

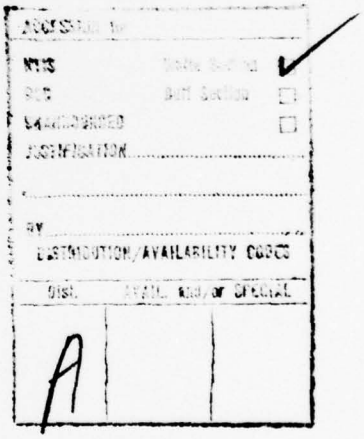

TABLE OF CONTENTS

1. INTRODUCTION

In this article we shall deal with the Wilson Cloud formed by low altitude nuclear explosions[1]. Despite the fact that it is a well-known phenomenon, we have found no detailed treatment of it in the literature. The basis of the effect is straightforward. During the weak shock phase of an explosion, over a certain volume, the pressure behind the shock front becomes less than ambient atmospheric pressure. Thus parcels of air passing through the shock undergo a sudden expansion and on occasion temporarily drive the relative humidity to supersaturation. Under these conditions the radii of water droplet aerosols present can grow many orders of magnitude, thereby momentarily forming a cloud in a region behind the advancing shock. We shall restrict the discussion here to maritime aerosols composed of salt solution droplets.

We shall demonstrate that (1) there is a threshold of ambient relative humidity for significant cloud formation independent of the explosion energy; and (2) over a wide range of explosion energies the maximum cloud droplet sizes are nearly independent of the ambient aerosol spectrum and may be scaled with the explosion energy.

In Section 2, below, we discuss the hydrodynamic flow behind the shock wave and its effect on the relative humidity which drives the cloud formation. In Section 3 we review droplet growth kinetics and the basis for droplet size scaling. Finally, we give in Section 4, a universal scaled formulation of droplet size and cloud location together with a discussion of the limitations on our approach.

2. SHOCK HUMIDITY PROFILES

We shall concern ourselves here with the time, t, history of relative humidity, S, and temperature, T (^{0}K), of an air parcel passing through the shock wave. The parcel shall be denoted by its initial altitude, z, and its radial distance r, from the explosion center. S is given by

$$S \equiv [X/(X + \varepsilon)]\ P/p_s \tag{2.1}$$

where P is the pressure; X is the absolute humidity (grams of water vapor per gram of dry air); ε is the specific gravity of water vapor relative to that of air (0.621); and $p_s(T)$ is the saturation vapor pressure

$$p_s(T) \equiv (3.53 \times 10^4 \text{ dynes cm}^{-2}) \exp\left[-(L\varepsilon/R_d)(1/T - 1/300)\right] \tag{2.2}$$

L is the heat of vaporization of water (2.42×10^{10} erg g^{-1}); R_d is the dry air gas constant (2.87×10^6 erg g^{-1} K^{-1}).

A crucial simplifying approximation results from neglecting the water condensation, ΔX, compared to X. X is typically of the order of 10^{-2} and for explosion energies of the order of 10 kt, ΔX is at worst 1% of X. (We assume throughout a typical maritime aerosol number density of 100 cm^{-3}). The heat of condensation associated with the ΔX gives a temperature deviation from adiabaticity

$$\Delta T = -(L/C_p)\Delta X \tag{2.3}$$

where C_p is the specific heat of air at constant pressure (1.05×10^7 erg g^{-1} K^{-1}). Using $\Delta X \sim 10^{-4}$ we find $\Delta T \sim 0.2$ K and $(\Delta S/S) = -17.45\ (\Delta T/T) + (\Delta X/X) \sim 1\%$ which represents the strength of the coupling between dry air shock hydrodynamics and cloud formation. Neglecting this coupling allows the use of existing dry air calculations of shock wave profiles for pressure and temperature. These calculations assume that the post shock wave flow is adiabatic, i.e.,

$$T = T_s(P/P_s)^{(\gamma-1)/\gamma};\ \gamma = 1.4 \tag{2.4}$$

where P_S and T_S are the pressure and temperature of the parcel immediately following the passage of the shock front. Energy scaling laws presented below indicate the limitations on the decoupling approximation.

Decoupling of the dry air shock flow from the cloud formation allows us to write

$$S(r, z, t) = S_0(z)\, M(r, z, t) \tag{2.5}$$

where

$$M = (P/P_0) \exp\{17.45 \left(\frac{300}{T_0} \frac{P_0}{P} - 1\right)\} \tag{2.6}$$

P_0, T_0, ρ_0, S_0 are respectively, the ambient pressure, temperature, density, and relative humidity of the parcel in question. M depends on (P/P_0) and (ρ/ρ_0). These ratios are functions of $\ell = (r/r_0)$ and $\tau = (t/t_0)$ only. Here r_0 and t_0 are the dynamic length and dynamic time of the explosion[2]:

$$r_0 \equiv (E/P_0)^{1/3}$$

and

$$t_0 \equiv E^{1/3} P_0^{-5/6} \rho_0^{1/2}$$

E is the hydrodynamic energy of the explosion. Figure 1 gives plots of the universal function $M(\tau, \ell)$ versus τ for various ℓ values ($T_0 = 288.15$ K is used). These curves are based on the numerical treatments of shock profiles due to Needham, et al[3]. Their work is in apparent agreement with that reported in Reference 2 and Reference 4.

As we shall see below significant cloud formation, i.e., large droplet growth, results only when the relative humidity in a parcel at ℓ is driven to supersaturation $S > 1.0$. Thus, from Equation (2.5) there is an energy independent threshold of ambient humidity $S_{th}(\ell)$ for cloud formation at each ℓ given by $M^*(\ell)^{-1} = (\max\{M(\tau,\ell)\})^{-1}$. Figure 2 plots $S_{th}(\ell)$ versus ℓ. ($\Delta\tau(\ell)$ is defined after Equation 4.2). We find from Figure 1, that, regardless of S_0, cloud formation can begin only after time $\tau \simeq 0.35$ and outside a radius $\ell \simeq 0.6$. We emphasize here

that cloud formation first begins during a period when neither strong shock (self-similar) theory nor weak shock (asymptotic) theory is valid. From $\tau \sim .03$ to $\tau \sim 1$ a numerical treatment of shock hydrodynamics is required. We note in passing that in the region of cloud formation, spatial motion of the parcel due to shock winds is generally small and of no interest to the problem. A striking feature apparent from Figure 2 is that if the ambient humidity is nowhere greater then 70% then no Wilson cloud of significance can form.

3. DROPLET GROWTH KINETICS

The equation of growth for a salt solution droplet, the principal constituent of maritime aerosols, is[5]

$$\bar{r}(d\bar{r}/dt) = [S(t) - S_{eq}(\bar{r},m)]/Y(T) \tag{3.1}$$

where S is the shock driven relative humidity in the air parcel containing the droplet as discussed above. $S_{eq}(\bar{r},m)$ is the equilibrium relative humidity for a droplet with radius $\bar{r}$, and salt mass m. Y(T) is a weakly temperature-dependent coefficient determined by the heat and water vapor diffusion rates in air. In c.g.s. units

$$S_{eq}(\bar{r},m) = \exp\left(2\sigma\varepsilon/\rho_L R_d T\bar{r}\right) - 3i\, mM/\pi\rho_L W\bar{r}^3 \tag{3.2}$$

$$Y(T) = (L\rho_L/KT)(L\varepsilon/(R_d T) - 1) + \rho_L R_d T/(D\varepsilon P_S(T))$$

$$(Y\ (300K) = 7.26 \times 10^5\ \text{sec/cm}^2) \tag{3.3}$$

where quantities not given previously are defined here:

ρ_L = density of liquid water = 1 g cm^{-3}
σ = surface of water = 72 dyne cm^{-1}
K = thermal conductivity of air = 2.5×10^3 erg cm^{-1} sec^{-1}
D = water vapor diffusivity in air = 2×10^{-1} cm^2 sec^{-1}
i = Van Hoff's constant = 2.7
M = molecular weight of water = 18
W = molecular weight of salt = 58

As an illustration of the droplet growth and evaporation cycle, Figure 3 considers five exemplary droplet species of salt mass m_i (grams) and relative population n_i (as suggested by Reference 5) contained in a typical shocked air parcel. (For this case E is of the order of 10 kt and $S_o \sim 0.89$). The relative humidity S seen by the dorplets is plotted versus their radii starting from their entrance to the shock until their

evaporation behind the advancing clouds. The $S_{eq}(\bar{r}, m_i)$ curves are also shown. Upon entering the shock wave a droplet quickly evaporates and, after a sudden drop in S, its nucleus returns to its equilibrium curve. It remains there until S is driven beyond supersaturation, at which point rapid droplet growth begins. Each species tagged by its initial mass is found to grow nearly to the same maximum radius. Such narrowing of the droplet radial spectrum is in common with droplet growth in thunderheads[5]. This feature, which we shall call universal growth, is particularly striking in Wilson cloud growth where the droplet size at maximum growth are independent of the ambient aerosol spectrum.

Universal growth may be understood by noting that for each droplet species, once S passes above unity, where significant growth results, $S_{eq}(\bar{r},m)$ for the resulting $\bar{r}$ is very nearly equal to unity and may be so replaced in Equation 3.1. This allows the growth equation to be rewritten in terms of scaled variables and the universal function $M(\tau,\ell)$ driving the relative humidity. We have then, independent of species, i.e., independent of m,

$$d((1/2)R^2(\tau,\ell)/d\tau \simeq (S_o(z)\, M(\tau,\ell) - 1) \tag{3.4}$$

where

$$\bar{r}^2(t,r,m) = R^2(\tau,\ell)\, t_o Y^{-1} \tag{3.5}$$

Y is nearly constant over the course of growth and evaporation and we use Y(300) as given above. At a given ℓ, cloud formation begins and maximum growth is obtained at the times for which $M(\tau,\ell) = S_o^{-1}$. We denote these times as $\tau_1^*(\ell)$ and $\tau_2^*(\ell)$ respectively. They may be easily read from Figure 1. Since droplets typically attain radial growths significantly larger than their ambient radii, a suitable initial condition for Equation 3.4 is

$$R^2\,(\tau_1^*(\ell),\ell) \simeq 0 \tag{3.6}$$

independent of species. No new length scale is introduced thereby and the solution to Equations 3.4 and 3.6 is therefore universal.

To clarify the meaning of universal scaled droplet growth (Equations 3.4, 3.5 and 3.6) note that they imply the following: if at a distance r and time t from an explosion of energy E the droplet radius in the Wilson

cloud is $\bar{r}$, then for explosion energy E', $\bar{r}' = \bar{r}(E'/E)^{1/6}$ at $r' = r(E'/E)^{1/3}$ and $t' = t\,(E'/E)^{1/3}$ assuming the same ambient humidity prevails. Furthermore the approximate cloud droplet size can be calculated entirely without regard to the ambient aerosol spectrum.

4. RESULTS OF SCALING AND UNIVERSAL DROPLET GROWTH

We present here scaled formulas for maximum droplet size as well as location contours of cloud formation and evaporation. For each ℓ value for distance from the explosion center, we may approximate that portion of the M function greater than unity as a parabola

$$M(\tau,\ell) \simeq (M^*(\ell) - 1)\ (1 - y^2) + 1 \tag{4.1}$$

where $M^*(\ell)$ is the maximum of M for the given ℓ (See Figure 2); and

$$y \simeq [(\tau - \tau_2) + (\Delta\tau/2)]/(\Delta\tau/2) \tag{4.2}$$

where $\Delta\tau(\ell) = \tau_2(\ell) - \tau_1(\ell)$ and τ_1 and τ_2 are the times at which M passes through unity.

Integrating the scaled droplet growth Equation 3.4, subject to the universal initial condition Equation 3.6, over the time such that $S_o M \geq 1.0$ (i.e., between $\tau_1 \geq \tau_1^*$ and $\tau_2 \leq \tau_2^*$) we find

$$R^2_{max}(\ell) = R^2(\tau_2^*(\ell),\ell) =$$

$$(4/3)\ \Delta\tau(\ell)\ \left[\left(\frac{S_o}{S_{th}(\ell)}\right) - 1\right]\ \left[\frac{1 - (S_{th}(\ell)/S_o)}{1 - S_{th}(\ell)}\right]^{1/2} \tag{4.3}$$

$\Delta\tau(\ell)$ is plotted in Figure 2 along with $S_{th}(\ell)$. $R^2_{max}(\ell)$ is plotted in Figure 4 for various ambient

By using the exact M functions to integrate Equation 3.4 beyond $\tau_2^*(\ell)$ to evaporation where R^2 returns to zero, we obtain the evaporation time $\tau_3^*(\ell)$. Figure 5 gives contours of cloud formation ($\tau_1^*(\ell)$), maximum growth ($\tau_2^*(\ell)$), and evaporation ($\tau_3^*(\ell)$), for various values of ambient relative humidity percentages ranging from 70% - 100%. Note that as the relative humidity approaches 100%, the cloud once formed at a given location ℓ, requires an increasingly longer time to evaporate. The contours may be read at constant τ to find the location of the outside and inside of the cloud, as well as the

ℓ value of maximum growth. Figure 4 and Equation 3.5 may then be used to find maximum droplet radius.

The scaling laws may be used to find the limits of validity for the approach taken here. We have noted in Section 2 that for E of the order of 10 kt and neglecting water condensation, ΔX results in errors of S of the order of 1%. Since droplet radii scale as $E^{1/6}$, ΔX scales as $E^{1/2}$. Thus for E of the order of 100 kt, the error in S would be of order 3% which is probably unacceptably large compared to a typical supersaturation (S-1) inside the cloud. Thus, for accurate results larger energies require a treatment which couples cloud formation to shock hydrodynamics, the simple scaling laws presented here being inadequate.

The universal droplet growth equations will also show breakdown for very low explosion energies such that the length scale introduced by the ambient droplet sizes becomes important. This is the case if the typical values of R^2_{max} (ℓ) given by Equation 4.2 or Figure 4 are not considerably larger than $R^2 \equiv \bar{r}_o^2\, t^{-1} Y$ where $\bar{r}_o(\bar{m})$ is the equilibrium radius of a representative droplet species at 100% relative humidity. Let us consider a median salt grain such as #3 of Figure 3 which has $\bar{r}_o = 4.5 \times 10^{-5}$ cm. For E = 10 kt this corresponds to $R^2_o \sim .5 \times 10^{-3}$. This is well above the typical values of R^2_{max} which in turn are conservatively of the order of .01. However, since R^2_o scales like $E^{-1/3}$ we expect our treatment to break down for E less than about 10^{-3}kt.

REFERENCES

1. Glasstone, S., Effects of Nuclear Weapons, U.S. Dept. of Defense, 1962.

2. Sedov, L.I., Similarity and Dimensional Methods in Mechanics, Academic Press (1959).

3. Needham, C.E., et al, "Nuclear Blast Standard (1 kt)", Air Force Weapons Laboratory Technical Report No. AFWL-TR-73-55 (April 1973).

4. Bethe, H.A., et al, "Blast Wave", Los Alamos Scientific Laboratory LA-2000 (1949).

5. Mason, J., The Physics of Clouds, Clarendon Press, Oxford, (1971).

FIGURE CAPTIONS

FIGURE 1: Universal shocked relative humidity multiplying function, M, versus dynamic time, τ, for air parcels at various dynamic lengths, ℓ, (curve labels).

FIGURE 2: Relative humidity threshold for cloud formation, $S_{th}(\ell)$, versus dynamic length ℓ; $M^*(\ell) = [S_{th}(\ell)]^{-1}$; pulse duration for $M > 1.0$, $\Delta\tau(\ell)$, versus dynamic length ℓ.

FIGURE 3: Droplet growth and evaporation curves in the relative humidity, S, and droplet radius, $\bar{r}$, plane. $S_{eq}(\bar{r}, m)$, the equilibrium curves are shown as dashed curves. The salt mass, m_i (grams), and relative number n_i, of the species are shown.

FIGURE 4: Square of the universal maximum droplet radius, $R^2_{max}(\ell)$, versus dynamic length, ℓ, for various ambient relative humidities.

FIGURE 5: Contours of cloud formation time, τ_1^*, time of maximum growth τ_2^*, and evaporation time, τ_3^*, versus dynamic length, ℓ, for various ambient relative humidities.

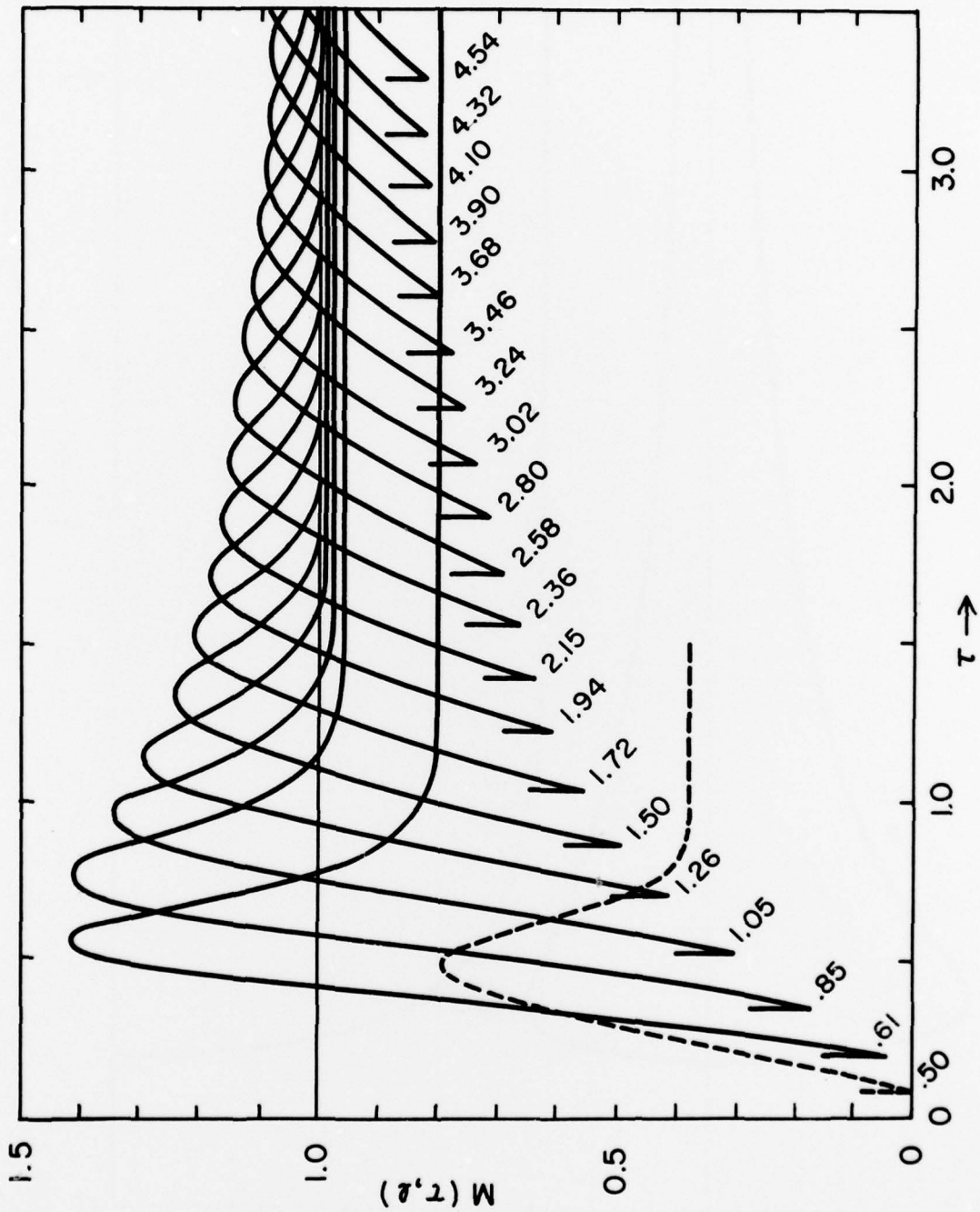
4.54
4.32
4.10
3.90
3.68
3.46
3.24
3.02
2.80
2.58
2.36
2.15
1.94
1.72
1.50
1.26
1.05
.85
.61
.50
0
1.0
2.0
3.0
τ →
M (τ, β)
1.5
1.0
0.5
0

FIGURE 1

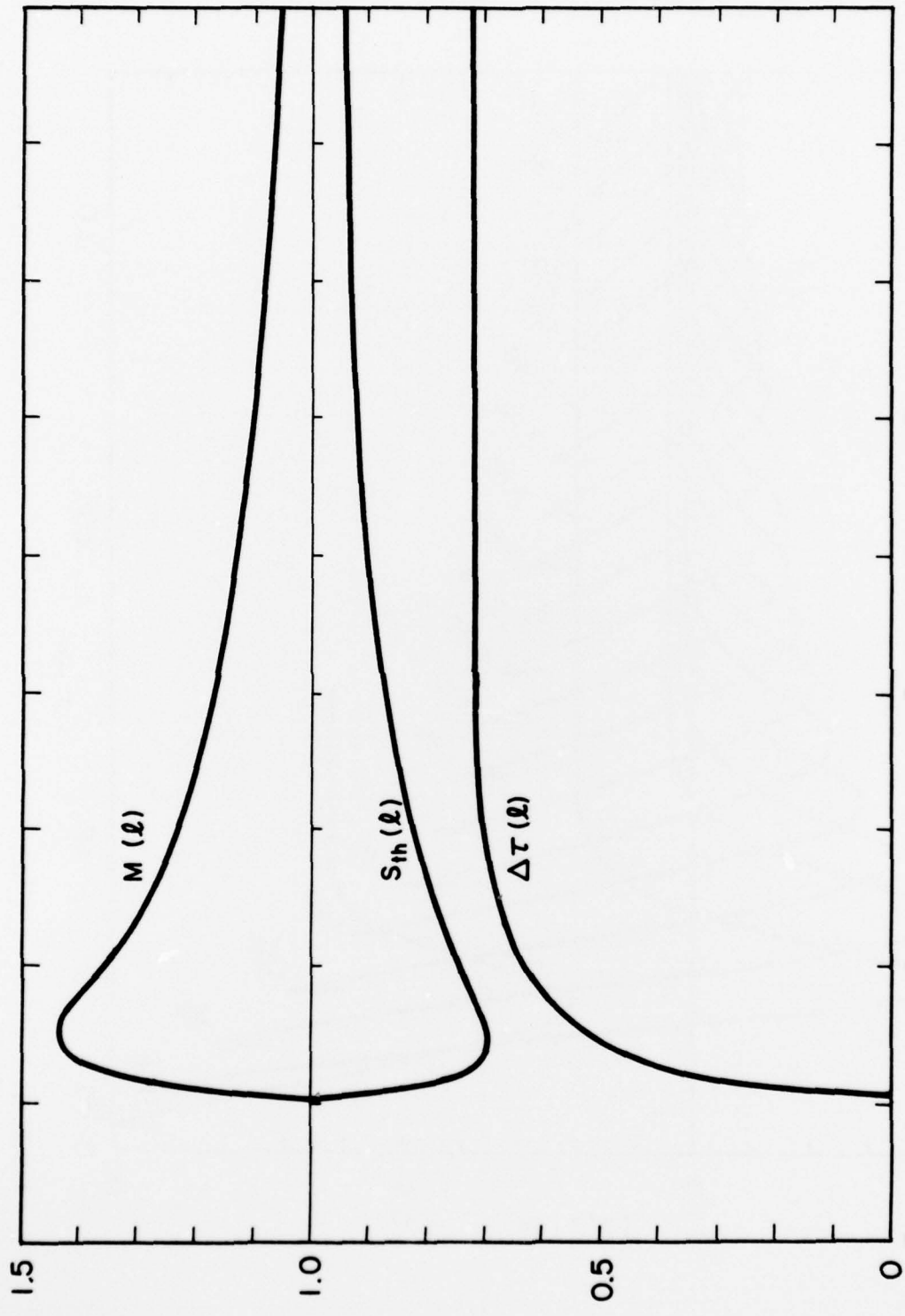

FIGURE 2

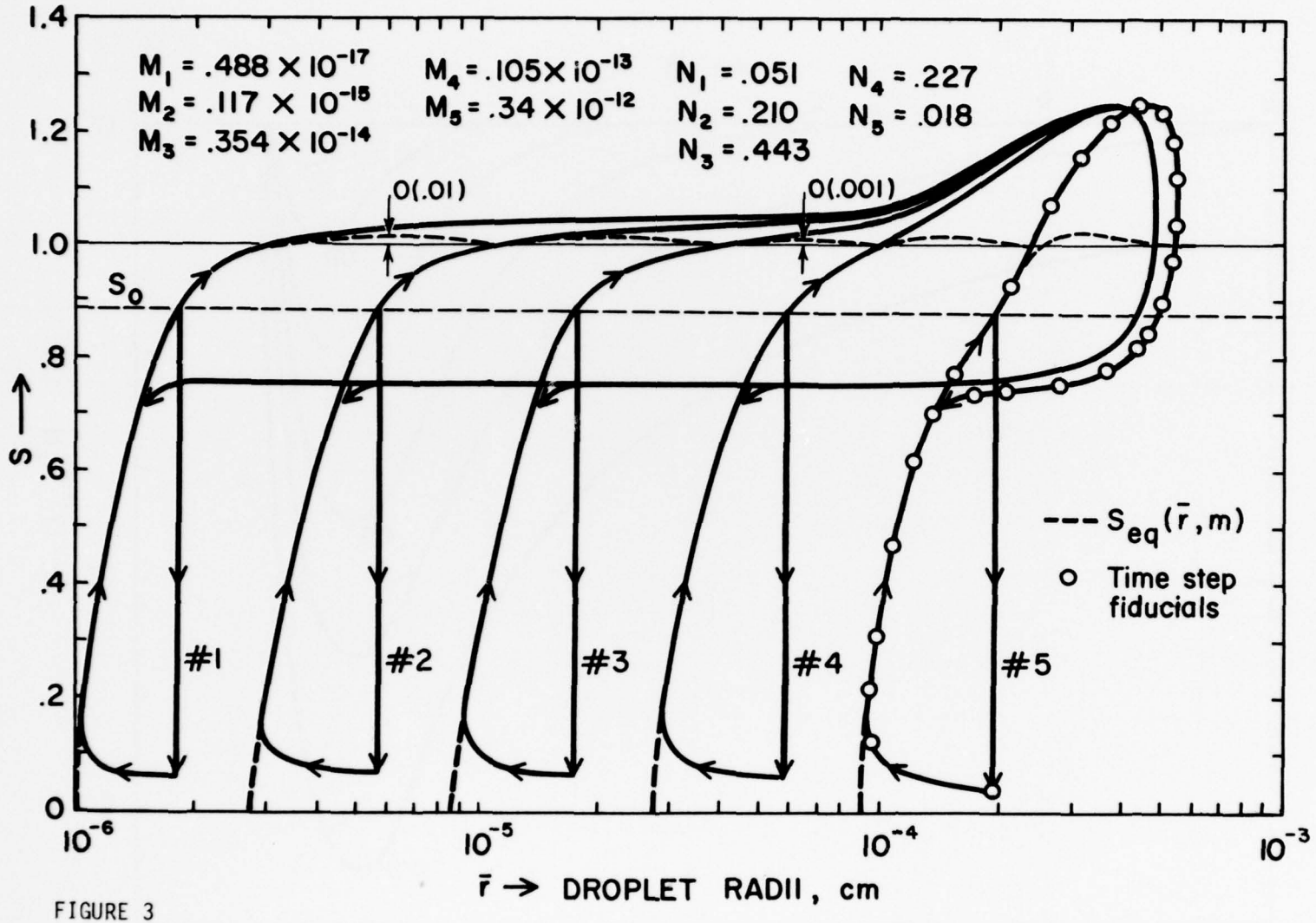
$M_1 = .488 \times 10^{-17}$
$M_2 = .117 \times 10^{-15}$
$M_3 = .354 \times 10^{-14}$
$M_4 = .105 \times 10^{-13}$
$M_5 = .34 \times 10^{-12}$
$N_1 = .051$
$N_2 = .210$
$N_3 = .443$
$N_4 = .227$
$N_5 = .018$
O(.01)
O(.001)
S_0
S
#1
#2
#3
#4
#5
$S_{eq}(\bar{r}, m)$
Time step fiducials
1.4
1.2
1.0
.8
.6
.4
.2
0
10^{-6}
10^{-5}
10^{-4}
10^{-3}
$\bar{r}$ → DROPLET RADII, cm

FIGURE 3

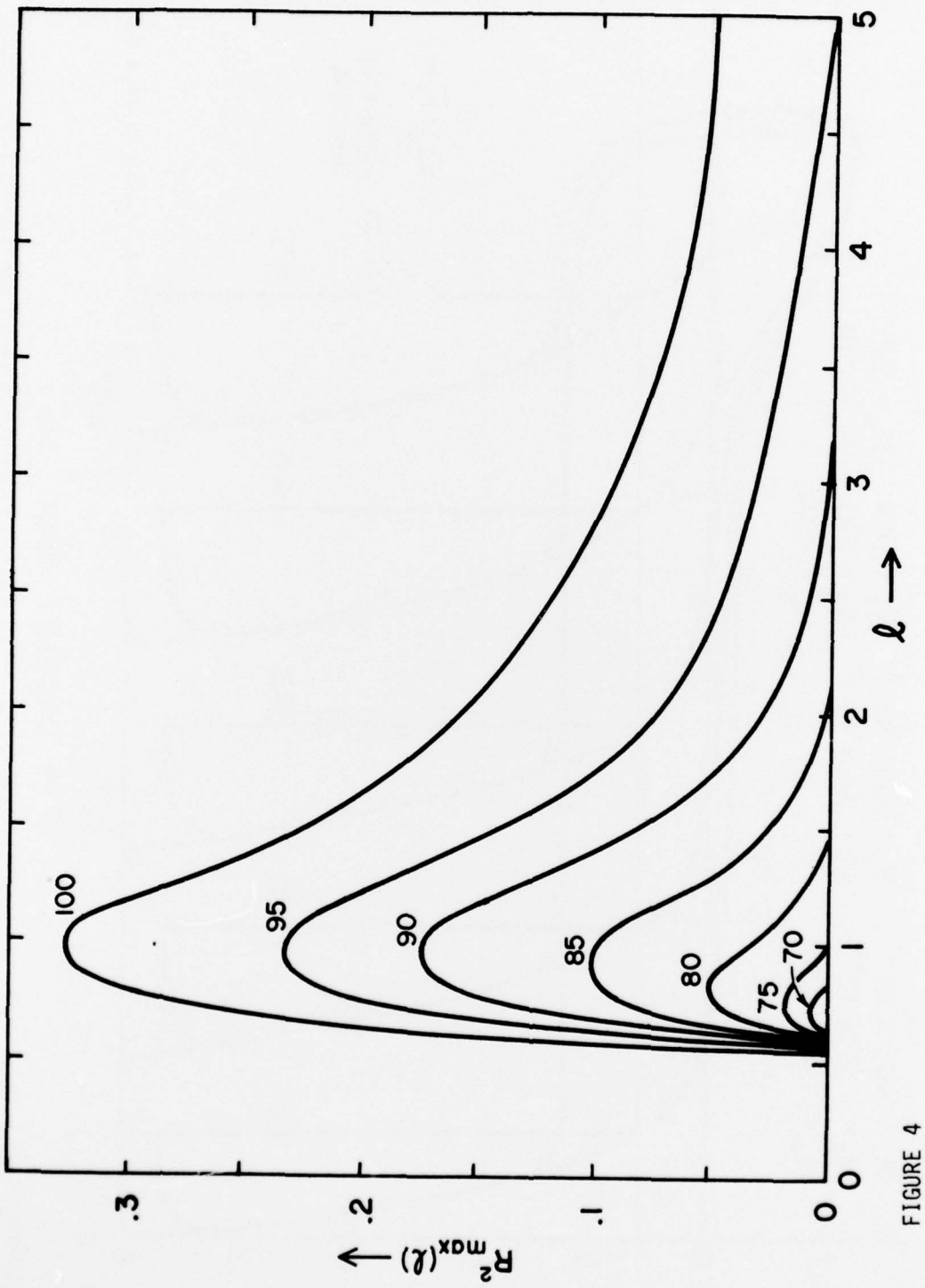

FIGURE 4

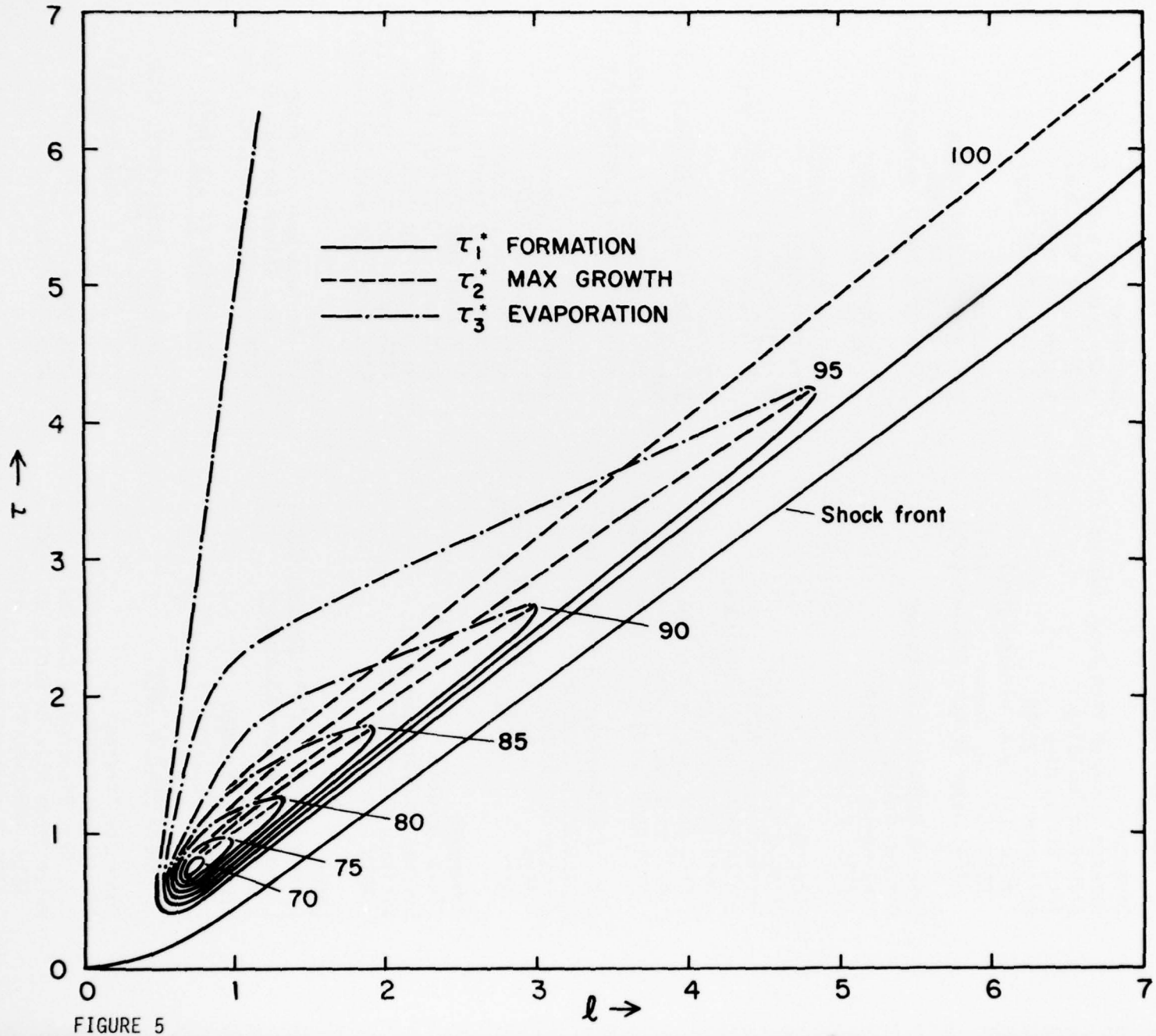
τ_1^* FORMATION
τ_2^* MAX GROWTH
τ_3^* EVAPORATION
100
95
90
85
80
75
70
Shock front
τ →
ℓ →
0
1
2
3
4
5
6
7

FIGURE 5

DISTRIBUTION LIST

DEPARTMENT OF DEFENSE

Director
Defense Advanced Rsch Proj. Agency
Architect Building
1400 Wilson Blvd.
Arlington, VA 22209
ATTN Ltc. W.A. Witaker (1cy)
ATTN STC J. Jenny (1cy)
ATTN Major Gregory Canavan (1cy)

Defense Documentation Center
Cameron Station
Alexandria, VA 22314
ATTN TC (12cy)

Director
Defense Nuclear Agency
Washington, DC 20305
ATTN STTL Tech Library (3cy)
ATTN STSI Archives (3cy)
ATTN RAAE Charles A. Blank (3cy)
ATTN RAAE Maj J Mayo (3cy)
ATTN RAAE Gordon K. Soper (1cy)

Dir. of Defense Rsch & Engineering
Department of Defense
Washington, DC 20301
ATTN Daniel Brockway (1cy)
ATTN Richard S. Ruffine (1cy)

Commander
Field Command
Defense Nuclear Agency
Kirtland AFB, NM 87115
ATTN FCPR (1cy)

Chief
Livermore Division Fld Command DNA
Lawrence Livermore Laboratory
P.O. Box 808
Livermore, CA 94550
ATTN FCPRL (1cy)

DEPARTMENT OF ARMY

Commander/Director
Atmospheric Sciences Laboratory
U.S. Army Electronics Command
White Sands Missile Range, NM 88002
ATTN DRSEL-BL-SY-S F.E. Niles (1cy)
ATTN E. Butterfield DRSEL-BL-SY-R (1cy)

Commander
Harry Diamond Laboratories
2800 Powder Mill Road
Adelphi, MD 20783
ATTN DRXDO-NP (2cy)

Commander
U.S. Army Nuclear Agency
Fort Bliss, TX 79916
ATTN ATCA-NAW J. Berberet (1cy)

DEPARTMENT OF NAVY

Chief of Naval Research
Navy Department
Arlington, VA 22217
ATTN Code 427 Cdr R.J. Oberle (1cy)

Commander
Naval Electronics Laboratory Center
San Diego, CA 92152
ATTN Code 2200 1 V.E. Hildebrand
ATTN Code 2200 I. Rothmuller (1cy)

Director
Naval Research Laboratory
Washington, DC 20375
ATTN Douglas P. McNutt (1)
ATTN Code 7127 Charles Y. Johnson (1)
ATTN Code 2027 Tech Lib (1)
ATTN Code 7700 Timothy P. Coffey (1)
ATTN Code 7701 Jack D. Brown (1)
ATTN Code 7750 D.F. Strobel (1)
ATTN Code 7750 Paul Julienne(1)

Commander
Naval Surface Weapons Center
White Oak, Silver Springs, MD 20910
ATTN Code WA501 Navy Nuc Pgms Off

DEPARTMENT OF AIR FORCE

AF Geophysics Laboratory, AFSC
Hanscom AFB, MA 01731
ATTN LKB K.S.W. Champion (1)
ATTN OP John S. Garing (1)
ATTN OPR A.T. Stair (1)
ATTN OPR H. Gardiner (3)

AF Weapons Laboratory, AFSC
Kirtland AFB, NM 87117

ATTN SUL (1)
ATTN Dyt Ltc Don Mitchell (1)

Commander
ASD
WPAFB, OH 45433
ATTN ASD-YH-EX Ltc Robert Leverette

SAMSO/SZ
Post Office Box 92960
Worldway Postal Center
Los Angeles, CA 90009
(Space Defense Systems)
ATTN SZJ Major Lawrence Doan (1)

U.S. ENERGY RESEARCH & DEV. ADMIN.

Division of Military Application
U.S. Energy Rsch & Dev Admin
Washington, DC 20545
ATTN DOC CON FOR Maj. D.A. Haycock (1)

Los Alamos Scientific Laboratory
P.O. Box 1663
Los Alamos, NM 87545
ATTN DOC CON FOR R.A. Jeffries (1)

OTHER GOVERNMENT

Department of Commerce
Office of Telecommunications
Institute for Telecom Science
Boulder, CO 80302
ATTN William F. Utlaut (1)
ATTN Glenn Falcon (1)

DEPARTMENT OF DEFENSE CONTRACTORS

Aerodyne Research, Inc.
Bedford Research Park
Crosby Drive
Bedford, MA 01730
ATTN F. Bien
ATTN M. Camac

Aerospace Corporation
P.O. Box 92957
Los Angeles, CA 90009
ATTN T. Taylor
ATTN R. Grove
ATTN R.D. Rawcliffe
ATTN Harris Mayer

University of Denver
Colorado Seminary
Denver Research Institute
P.O. Box 10127
Denver, CO 80210
ATTN Sec Off for Mr. Van Zyl (1)
ATTN Sec Off for D. Murcray (1)

General Electric Company
Tempo-Center for Advanced Studies
816 State Street (P.O. Drawer QQ)
Santa Barbara, CA 93102
ATTN DASIAC Art Feryok (5)
ATTN Warren S. Knapp (1)

General Research Corporation
P.O. Box 3587
Santa Barbara, CA 93105
ATTN John Ise, Jr. (1)

Geophysical Institute
University of Alaska
Fairbanks, AK 99701
ATTN T.N. Davis (1)
ATTN Neal Brown (3)

Honeywell Incorporated
Radiation Center
2 Forbes Road
Lexington, MA 02173
ATTN W. Williamson (1)

Institute for Defense Analyses
400 Army-Navy Drive
Arlington, VA 22202
ATTN Ernest Bauer (1)
ATTN Hans Wolfhard (1)

Lockheed Missiles and Space Company
3251 Hanover Street
Palo Alto, CA 94304
ATTN J.B. Cladis Dept 52-12 (1)
ATTN J.B. Reagan D/52-12 (1)
ATTN Billy M. McCormac D/52-54 (1)
ATTN Tom James
ATTN Robert D. Sears D/52-14
ATTN John Kumer
ATTN Martin Walt Dept 52-10
ATTN Richard G. Johnson Dept 52-12

Mission Research Corporation
735 State Street
Santa Barbara, CA 93101
ATTN P. Fischer
ATTN D. Archer

Photometrics, Inc.
442 Marrett Road
Lexington, MA 02173
ATTN Irving L. Kofsky

Physical Dynamics, Inc.
P.O. Box 1069
Berkeley, CA 94701
ATTN Joseph B. Workman

Physical Sciences, Inc.
30 Commerce Way
Woburn, MA 01801
ATTN Kurt Wray

R&D Associates
P.O. Box 9695
Marina Del Rey, CA 90291
ATTN Forrest Gilmore
ATTN Robert E. Lelevier

R&D Associates
1815 N. Ft. Myer Drive
11th Floor
Arlington, VA 22209
ATTN Herbert J. Mitchell

Rand Corporation
1700 Main Street
Santa Monica, CA 90406
ATTN James Oakley

Science Applications, Inc.
P.O. Box 2351
La Jolla, CA 92038
ATTN Daniel A. Hamlin

Space Data Corporation
1331 South 26th Street
Phoenix, AZ 85034
ATTN Edward F. Allen

Stanford Research Institute
333 Ravenswood Avenue
Menlo Park, CA 94025
ATTN Walter G. Chestnut
ATTN M. Baron
ATTN Ray L. Leadabrand

Stanford Research Institute
1611 North Kent Street
Arlington, VA 22209
ATTN Warren W. Berning

Technology International Corp.
75 Wiggins Avenue
Bedford, MA 01730
ATTN W. P. Boquist

Utah State University
Logan, UT 84321
ATTN Kay Baker
ATTN D. Burt
ATTN C. Wyatt

Visidyne, Inc.
19 Third Avenue
Northwest Industrial Park
Burlington, MA 01803
ATTN W. P. Reidy
ATTN J. W. Carpenter
ATTN T. C. Degges

☆U.S. GOVERNMENT PRINTING OFFICE: 1977 700-002/90